Bioorganic & Medicinal Chemistry 16 (2008) 8098–8108

Contents lists available at ScienceDirect

Bioorganic & Medicinal Chemistry

journal homepage: www.elsevier.com/locate/bmc

Molecular modeling and dynamics studies of Shikimate Kinase from *Bacillus anthracis*

Ivani Pauli [a], Rafael Andrade Caceres [a,b], Walter Filgueira de Azevedo Jr. [a,*]

[a] *Faculdade de Biociências, Laboratório de Bioquímica Estrutural, Pontifícia Universidade Católica do Rio Grande do Sul, Av. Ipiranga, 6681, Porto Alegre, 90619-900 Rio Grande do Sul, CEP, Brazil*
[b] *Programa de Pós Graduação em Medicina e Ciências da Saúde, Pontifícia Universidade Católica do Rio Grande do Sul, Porto Alegre, RS, Brazil*

ARTICLE INFO

Article history:
Received 18 June 2008
Revised 17 July 2008
Accepted 19 July 2008
Available online 25 July 2008

Keywords:
Molecular dynamics
Molecular modeling
Shikimate Kinase
Bacillus anthracis
Bioterrorism

ABSTRACT

Bacillus anthracis has been used as weapon in bioterrorist activities, with high mortality, despite anti-microbial treatment, which strongly indicates a need of new drugs to treat anthrax. Shikimate Pathway is a seven-step biosynthetic route which generates chorismic acid. The shikimate pathway is essential for many pathological organisms, whereas it is absent in mammals. Therefore, these enzymes are potential targets for the development of non-toxic anti-microbial agents and herbicides and have been submitted to intensive structural studies. Shikimate Kinase is the fifth enzyme of shikimate pathway and catalyzes the specific phosphorylation of the 3-hydroxyl group of shikimate using ATP as a co-substrate, resulting in shikimate-3-phosphate and ADP. The present work describes for the first time a structural model for the Shikimate Kinase from *B. anthracis* using molecular modeling approach and molecular dynamics simulations. This study was able to identify the main residues of the ATP-binding and the shikimate pockets responsible for ligand affinities. Analysis of the molecular dynamics simulations indicates the structural features responsible for the stability of the structure. This study may help in the identification of new inhibitors for this enzyme.

1. Introduction

Bacillus anthracis is an animal pathogen known since 1887, when was described by Koch and L. Pasteur. *B. anthracis* is the etiological agent of anthrax. Like all the members of the genus *Bacillus*, it is a Gram-positive bacterium, which produces spores in unfavorable environment conditions. Its natural habitat is the soil, where it can be viable for decades. The anthrax is a disease that occurs primary in herbivores. Humans are infected by exposure to sick animals or derivate products of these animals.[1] The infection occurs by a contamination with bacteria spores that can go into the organism through three ways: inoculation, inhalation and ingestion.[2]

Recent events have strongly indicated the potential of *B. anthracis* as an agent of bioterrorism.[3] In October 2001, four inhalational anthrax cases in the United States were identified in a large mail processing and distribution center in Washington, DC, after envelopes containing *B. anthracis* spores were processed.[4,5] The anthrax is related with high mortality, despite anti-microbial treatment and therapy.[6] Therefore, there is an urgent need of new therapies to treat anthrax. Among potential targets, to be used on the development of drugs against bacterial diseases 2-*trans*-enoyl-ACP (CoA) reductase[7–12] and enzymes from shikimate pathway (SP) deserve special attention.[13–17]

In plants and microorganisms, all the key aromatic compounds, involved on the primary metabolism, are produced by SP. It is a seven-step biosynthetic route which generates chorismic acid (the major branch point in the synthesis of aromatic amino acids, ubiquinone, and secondary metabolites) from phosphoenol pyruvate and erythrose-4-phosphate. This pathway is essential for algae, higher plants, bacteria, fungi, apicomplexan parasites, whereas it is absent in mammals.[18] Therefore, these enzymes are potential targets for the development of non-toxic anti-microbial agents[19] and herbicides.[20] Several enzymes of the SP have been submitted to structural studies.[21–27] Knowledge of three-dimensional structures will undoubtedly aid the design of useful inhibitors.

The object of our study is the fifth enzyme of the SP, Shikimate Kinase (SK), which catalyzes the specific phosphorylation of the 3-hydroxyl group of shikimate using ATP as a co-substrate, resulting in shikimate-3-phosphate (S3P), and ADP.[28]

It has been demonstrated that the gene aroK, is essential for bacteria, such as *Mycobacterium tuberculosis*.[29] In addition, this gene is not present in human genome, therefore we chose it as a target for inhibitor development.

SK belongs to the same structural family of nucleoside monophosphate (NMP) kinases. A characteristic feature of the NMP kinases is that they undergo large conformational changes during catalysis.[30]

* Corresponding author. Tel.: +55 51 33203500.
E-mail address: walter.junior@pucrs.br (W.F. de Azevedo).

0968-0896/$ - see front matter © 2008 Elsevier Ltd. All rights reserved.
doi:10.1016/j.bmc.2008.07.051

Previously *Mt*SK and other NMP kinases were classified as consisting of three domains including an SB (Shikimate-Binding) or NMP-binding domain, a CORE domain and the LID domain. Based on analysis of global movements accompanying conformational changes in agreement with the sequence of ligands entrance, four domains were identified in *Mt*SK,[31] the Extended Substrate-Binding (ESB) site, the Nucleotide-Binding (NB) site, the LID domain and the Reduced Core (RC) domain. The ESB domain comprises residues 31–91 in *Ba*SK and includes the SB sub-domain (residues 31–60). NB site contains the phosphate-binding (P-) loop (Walker-A motif, 8–16), the AB-loop (145–152) and the segment 100–109 including α6 (103–109). The LID domain is composed by the residues from 111 to 123. The remaining part of the molecule forms the RC domain. Fig. 1 shows these domains for *Ba*SK.

The three-dimensional structure of SK from *B. anthracis* (*Ba*SK) was modeled in both *apo* and complexed forms corresponding to individual steps in the enzymatic reaction. We used as templates crystallographic structures of SK from *M. tuberculosis* (*Mt*SK) which include the (unliganded) *apo*-form of the enzyme, binary complexes of the enzyme with MgATP and with shikimate (SKM), and a ternary complex with the products S3P and ADP.

Considerable progress in computer simulation has been made in recent years. Improvement in force fields, simulation techniques, protocols and increasing computer power are playing prominent roles in a wide area of research, including molecular dynamics (MD). The use of MD simulation allows monitoring the dynamics of individual atoms thereby giving a unique insight into the molecule behavior that cannot be easily extracted from laboratory experiments.

MD simulations are becoming a powerful tool for analyzing biological processes and proving to be a reliable way to understand the static and dynamic aspects in solution, avoiding difficulties that can occur in a crystalline environment.[32]

The present work discusses the structural features of the homology models obtained for *Ba*SK, the structural stability assessed by MD simulation and the potential of these structures on the studies of new inhibitors that may generate a new generation of drugs against *B. anthracis*.

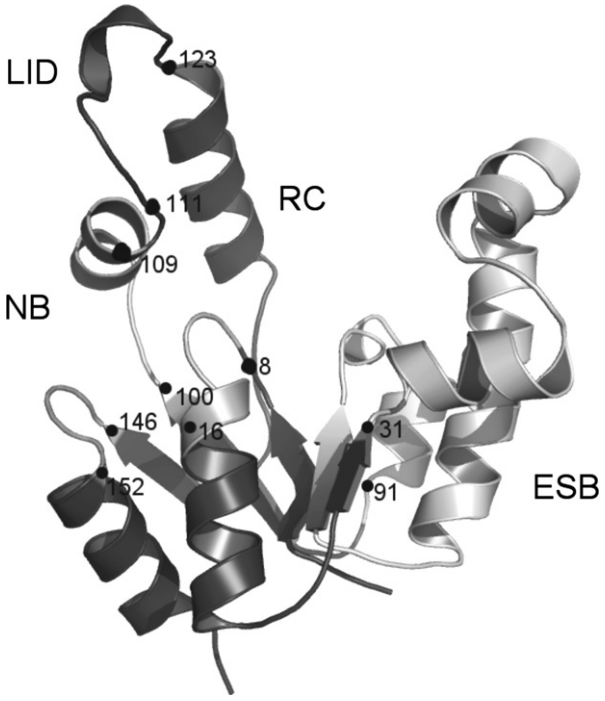

Figure 1. This image illustrates the 4 domains for *Ba*SK. The residues at both ends are indicated. Image generated by Pymol.[58]

2. Results and discussion

2.1. Quality of the models

There is no crystallographic structure available for *Ba*SK. The sequence of *Mt*SK shows 32% of identity with the sequence of *Ba*SK. This percentage of primary sequence identity indicates that the crystallographic structures of *Mt*SK are fair models to be used as templates for modeling of *Ba*SK. Furthermore, there are several binary complexes between *Mt*SK and their ligands (SKM, ATP, ADP, and S3P), which make available templates to model binary complexes of *Ba*SK against these ligands. The atomic coordinates of crystallographic structures of templates were used as basic models for modeling of the *Ba*SK. The analysis of the Ramachandran diagram $\phi - \psi$ plots was used to compare the overall stereochemical quality of the *Ba*SK structures against those of the templates solved by biocrystallographic methods. The homology models present over 89.3% of the residues in the most favorable regions (Table 1).

2.2. Overall description

*Ba*SK is an α/β protein consisting of a mixed β-sheet surrounded by α helices. A central five stranded parallel β-sheet (β1–β5) presents the strand order 2, 3, 1, 4, and 5 that consist of residues 29–31, 73–75, 4–7, 96–100, and 143–146, respectively. The β-strands are flanked on either side by α helices (α1 and α8 on one side, α4, α5, and α7 on the other). The residues making up the helices are 14–25, 32–40, 44–51, 53–69, 84–90, 103–110, 122–134, and 152–163. Fig. 2 shows a schematic diagram of the *Ba*SK structure, with SKM and ADP bound to the structure.

The *Mt*SK structure consists of 176 amino acids with a molecular weight of 18,583.3 Da and a theoretical p*I* of 10.56. *Ba*SK consists of 165 amino acids with a molecular weight of 19,130.8 Da and a theoretical p*I* of 5.38. Analysis of the structures of the SKs shows that some mutations were observed in both ATP- and SKM-binding sites. These differences are shown in the primary sequence alignment of *Ba*SK and *Mt*SK (Fig. 3).

However, these mutations do not influence significantly in the affinity of the ligands against *Ba*SK. The pK_ds values, which indicate the affinity of shikimate and ADP/ATP to the proteins *Mt*SK and *Ba*SK are shown in Table 2 We can observe that the *Ba*SK models values do not change significantly from the templates (*Mt*SK).

Fig. 4 shows the superposition of *Ba*SK against *Mt*SK.

2.3. Domain motions

Previous studies based on high resolution crystal structures of *Mt*SK that corresponds to individual steps in the enzymatic reaction show that the random sequential binding of SKM and nucleotides is associated with domain movements. Fig. 5 shows the models obtained for *Ba*SK binary complexes that were modeled with the enzyme in a number of liganded states, including binary complexes of *Ba*SK with SO_4 or MgADP, and ternary complexes of *Ba*SK with shikimate (SKM) as one ligand and SO_4, ADP or MgADP as a second ligand. The global motions which are associated with the sequential binding for *Ba*SK are described in the following with respect to the RC domain.

The binding of nucleotides, ADP or ATP, induces a rotational movement of the NB domain (Fig. 6). The binding of SKM causes rotation of the ESB domain.

Previous studies indicate that a third type of global motion causing the LID to flap over the active site is associated with the binding of the first substrate, independent of whether it is shikimate or a nucleotide. For the LID, we observed two different confor-

Table 1
This table shows the percentage of residues of *Mt*SK (templates) and *Ba*SK (models) in each of the Ramachandran plot regions

Enzyme (PDB access code)	Most favorable region[a] (%)	Additional allowed region[a] (%)	Generously allowed region[a] (%)	Disallowed region[a] (%)
*Mt*SK (1WE2)	92.7	6.6	0.7	0.0
*Ba*SK (template 1WE2)	90.7	7.3	0.7	1.3
*Mt*SK (2IYU)	97.1	2.9	0.0	0.0
*Ba*SK (template 2IYU)	92.0	6.7	1.3	0.0
*Mt*SK (2IYV)	96.6	3.4	0.0	0.0
*Ba*SK (template 2IYV)	92.0	4.7	2.7	0.7
*Mt*SK (2IYW)	96.6	3.4	0.0	0.0
*Ba*SK (template 2IYW)	92.0	5.3	2.0	0.7
*Mt*SK (2IYS)	97.9	2.1	0.0	0.0
*Ba*SK (template 2IYS)	92.0	5.3	2.0	0.7
*Mt*SK (2IYR)	95.9	4.1	0.0	0.0
*Ba*SK (template 2IYR)	90.7	8.0	1.3	0.0
*Mt*SK (2IYQ)	98.6	1.4	0.0	0.0
*Ba*SK (template 2IYQ)	90.7	6.7	2.0	0.7
*Mt*SK (2IYY)	96.4	3.6	0.0	0.0
*Ba*SK (template 2IYY)	90.7	7.3	1.3	0.7
*Mt*SK (2IYZ)	96.4	3.6	0.0	0.0
*Ba*SK (template 2IYZ)	89.3	10.0	0.0	0.7

[a] The analysis of the Ramachandran diagram $\phi - \psi$ plots was used to compare the overall stereochemical quality of the *Ba*SK structures against those of the templates solved by biocrystallographic methods.

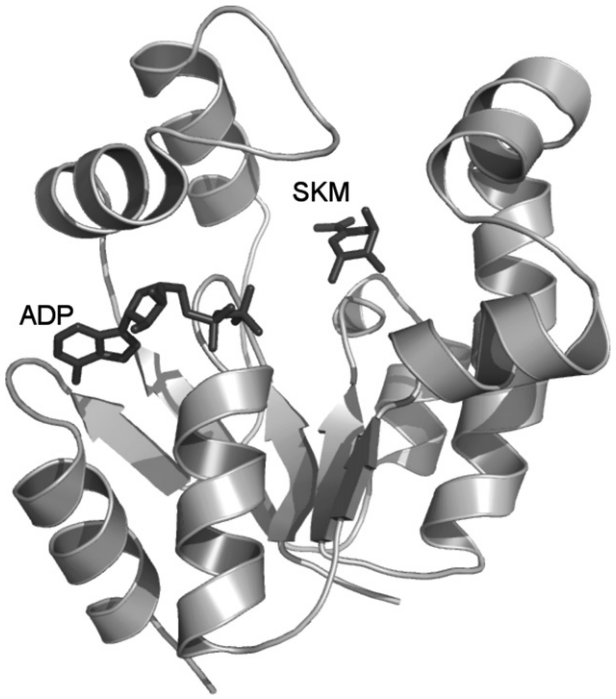

Figure 2. Tertiary structure of the *Ba*SK. The structure is presented as a ribbon diagram. The structure contains a central five stranded parallel β-sheet flanked on either side by α helices. The ligands SKM and ADP are bound to the protein. The image was generated using Pymol.[58]

mations before the closure (Fig. 7), indicating the high flexibility of this domain.

2.4. Shikimate binding

The substrate shikimate binds to a pocket formed by the conserved residues Asp33, Arg57, Gly78 and Gly79, and Arg135 (Fig. 8). The residues involved in the ADP/ATP- and SKM-binding sites for each binary complex are shown in Table 3. Analyzing all the structures we could see that approximately 65% of the residues involved in the binding pocket are conserved in all SKs. The superposition of the active sites of SKs from *B. anthracis* and *M. tuberculosis* give us a value of 0.36 Å, indicating that they are very similar to each other. We superposed the C-α of the residues that compose the shikimate-binding site which are Asp34, Arg58, Glu61, Gly79, Gly80, Gly81, and Arg136 for *Mt*SK and Asp33, Arg57, Glu60, Glu77, Gly78, Gly79, and Arg135 for *Ba*SK. The shikimate adopts essentially the same orientation in all complexes of *Ba*SK.

The intermolecular hydrogen bonds between *Ba*SK and SKM are described in Table 4. Most of the intermolecular hydrogen bonds observed in the binary complex *Mt*SK and SKM are conserved in *Ba*SK.

Experimental results for *Mt*SK suggest that shikimate binding to the enzyme involves two subsequent steps. In a first step, the substrate attaches to its binding site in its final orientation. In the absence of molecular packing interactions stabilizing this intermediate state, LID closure follows as a second step.[9]

2.5. Nucleotide binding

The binding of ATP or ADP to *Ba*SK involves interactions with the P-loop (residues 1–14 in *Ba*SK), the AB-loop (residues 146–152 in *Ba*SK), and α6 (residues 103–109 in *Ba*SK), all three motifs being conserved in SKs. Similar as in the case of shikimate binding, LID closure appears to follow nucleotide binding as a subsequent step.[9] The intrinsic conformation of the P-loop is well preserved in all *Ba*SK structures containing a nucleotide or sulfate that interacts with the P-loop. In particular, it is not affected by the binding of shikimate or shikimate-3-phosphate. Fig. 9 shows the active site of ATP in *Ba*SK. Around 30% of the residues involved in this active site are conserved in all SKs. The *Mt*SK nucleotide-binding site comprises the residues Lys15, Ser16, Thr17, Asp32, Asp34, Arg110, Arg117, Val148, Asp149, Thr150, Asn151, Arg152, Arg153, Asn154, and Pro155. The correspondents for *Ba*SK are Lys14, Thr15, Thr17, Asp31, Asp33, Arg109, Arg116, Ile145, Asp146, Thr147, Thr148, Asn149, Lys150, Ser151, and Val152. Some of these residues such as Lys14, Asp33, and Arg109 are conserved in bacterial SKs. The intermolecular hydrogen bonds between *Ba*SK and ADP/ATP are shown in supplementary material. Most of the intermolecular hydrogen bonds observed in the binary complex *Ba*SK structure are conserved in *Mt*SK.

2.6. Attempts to confirm the pK_d results

In order to confirm our results obtained for the affinities (pK_d values) of both ATP/ADP and SKM against *Ba*SK, we used the data from BRENDA (BRaunschweig ENzyme DAtabase).[33] There are K_m values for SK from the organisms *B. anthracis*, *Escherichia coli*,

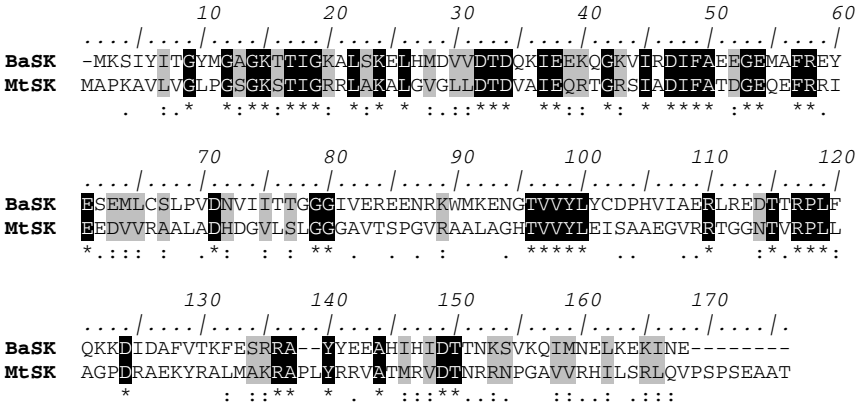

Figure 3. Sequence alignment for *Mt*SK and *Ba*SK. The alignment was performed using ClustalW and edited with BioEdit. (∗) and black boxes indicate positions which have a single fully conserved, (:) and gray boxes indicate that one of the following 'strong' groups is fully conserved, and (.) indicates that one of the following 'weaker' groups is fully conserved.

Table 2
pKd values that indicate the affinity of the ligand against the proteins *Mt*SK (templates) and *Ba*SK (models)

Enzyme (PDB access code)/ligand	ADP	SKM	ATP	S3P
*Mt*SK (1WE2)	5.6 (6.7)	4.8 (3.2)		
*Ba*SK (template 1WE2)	3.3 (8.6)	3.7 (6.4)		
*Mt*SK (2IYU)	5.4 (6.8)			
*Ba*SK (template 2IYU)	5.4 (7.3)			
*Mt*SK (2IYV)	5.7 (7.3)			
*Ba*SK (template 2IYV)	5.5 (7.3)			
*Mt*SK (2IYW)			5.7 (9.8)	
*Ba*SK (template 2IYW)			5.7 (8.2)	
*Mt*SK (2IYS)		5.0 (3.25)		
*Ba*SK (template 2IYS)		5.0 (4.8)		
*Mt*SK (2IYR)		4.9 (5.0)		
*Ba*SK (template 2IYR)		4.7 (4.4)		
*Mt*SK (2IYQ)	5.5 (7.6)	5.3 (4.5)		
*Ba*SK (template 2IYQ)	5.5 (7.9)	5.3 (6.1)		
*Mt*SK (2IYY)				5.2 (6.7)
*Ba*SK (template 2IYY)				5.3 (7.2)
*Mt*SK (2IYZ)	5.5 (8.3)			5.2 (4.5)
*Ba*SK (template 2IYZ)	5.4 (7.9)			5.3 (7.7)

All values are in pKd units.
In parentheses we present the values obtained with PEARLS.

Erwinia chrysanthemi, and *Methanococcus jannaschii* for ATP. To calculate the pK_d values we modeled the structures of SKs from these organisms with the ligands ATP and SKM using molecular modeling approach. As templates we used the structures deposited in the Protein Data Bank, with PDB access codes 1WE2, 1U8A and 2IYW in agreement with the molecular modeling procedure described in materials and methods. In a second moment, the programs XSCORE[34] and PEARLS[35] were used to evaluate the binding affinity of the ligands ATP/ADP and SKM against these SK structures. The calculated pK_d values are shown in Table 5.

Comparing the results obtained with XSCORE and PEARLS against experimental determined affinities, we can see that the pK_d values obtained by using PEARLS are slightly closer to the experimental ones, however, they can be used only for a qualitative analysis. Using PEARLS results we may suggest that SKM present higher affinity for SK from *B. anthracis*. This result is also observed using XSCORE. The high affinity of *Ba*SK for SKM is probably due to the higher number of hydrogen bonds between *Ba*SK and SKM when comparing with the other three enzymes (Table 6). *E. coli* presents the same number of intermolecular hydrogen bonds that *B. anthracis*; however, the intensity of electrostatic interactions seems to be lower due to the hydrogen bonds distance to be near to the cut off (~3.4 Å).

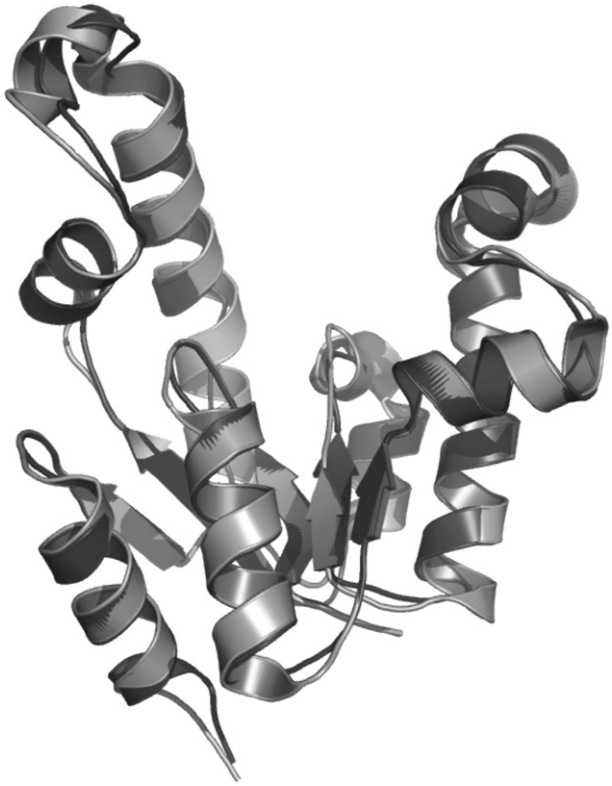

Figure 4. This figure illustrates the superposition of *Mt*SK (light gray) against *Ba*SK (dark gray). The image was generated using Pymol.[58]

In order to estimate the solvent accessible surface (ASA) and contact surface of the proteins cited above, we had performed analysis using AREAIMOL,[36] which is a program from the CCP4 package (Collaborative Computational Project, Number 4, 1994),[37] using default settings. The result does not show a correlation between the contact surface and the highest pK_d value for *Ba*SK. However, for *E. coli* this relation can be observed (Table 6). Nevertheless, contact surface contributes to increase protein–ligand affinity, as can be observed in the empirical scoring functions employed in the programs XSCORE and PEARLS.[34,35]

We used only the results for the ligand SKM because the ATP phosphate charges do not give us good results using PEARLS. The results for *B. anthracis* can be confirmed by enzymatic methods.

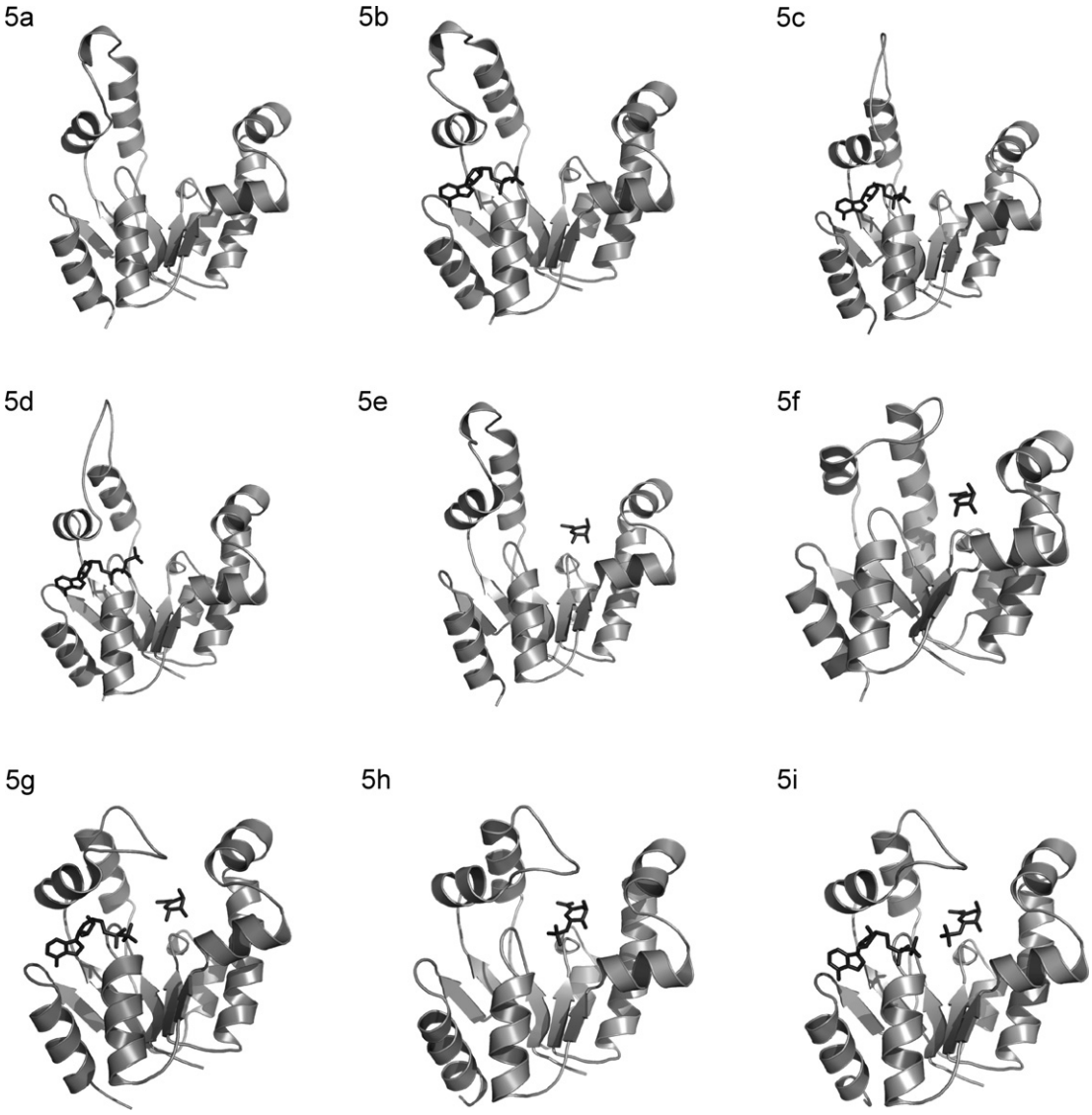

Figure 5. Representation of the models obtained for *Ba*SK binary complexes that were modeled with the enzyme in a number of liganded states. (**5a**) *Ba*SK(apo) with the LID in open(A) conformation; (**5b**) *Ba*SK:ADP LID with the LID in open(A) conformation; (**5c**) *Ba*SK:ADP with the LID in open(B) conformation; (**5d**) *Ba*SK:MgATP with the LID in open(B) conformation; (**5e**) *Ba*SK:SKM with the LID in open(A) conformation; (**5f**) *Ba*SK:SKM with the LID in closed conformation; (**5g**) *Ba*SK:SKM:ADP with the LID in closed conformation; (**5h**) *Ba*SK:S3P:SO_4 with the LID in closed conformation; (**5i**) *Ba*SK:S3P:ADP with the LID in closed conformation. The images were generated using Pymol.[57]

2.7. Molecular dynamics simulation

The root mean square deviation (RMSD) from the starting structure is an important criterion for the convergence of the protein system. The RMSD values of all Cα of BaSK (Open (System 1) and Closed (System 2) LID domain) and BaSK:SKM:ADP (System 3) structures are shown in Fig. 10, demonstrating that the 4 ns of simulation system appear to have been stabilized after 1000 ps of equilibration. Furthermore, the RMSD for the system 1 is higher than other systems (3.1 ± 0.5 Å), the system 2 presents slightly larger (2.6 ± 0.4 Å) than that for the system 3 (2.3 ± 0.4 Å), which indicates that the stability of *Ba*SK decreases upon binding the ligand.

Rg (Radius of gyration) as a function of time is shown in Fig. 11. Unfolding is often revealed by an increase of Rg. The mean values of the Rg averaged over the period from 0 to 4 ns were determined (16.0 ± 3.5, 15.7 ± 1.1, and 15.6 ± 1.2 for the systems 1, 2, and 3, respectively), remaining essentially constant after 2000 ps for those systems, suggesting that the molecular conformation was significantly preserved as a whole.

2.8. Principal component analysis

To support our results and investigate the most significant collective modes of motion occurring during the simulations of the uncomplexed and complexed *Ba*SK, the covariance matrix corresponding to the Cα-atom coordinates was calculated and PCA was performed. By diagonalizing the covariance matrix, the anharmonic and large-scale motions of the protein are isolated from the mostly harmonic and small-scale motions. Because the large-scale anharmonic motions in the essential subspace are often correlated to the vital functions of the protein, we only focus on these movements. The 3*N* eigenvalues (495 eigenvalues) of the covariance matrix were ranked in a decreasing order of magnitude (data not shown). Ninety-two percent of the total positional fluctuations are described by the first 50 eigenvectors of both models (data not shown), but different from the usual case, in which the first 10 eigenvectors represent ~95% of the total motion for the other protein.[38] This indicates that the fluctuations in *Ba*SK are more complicated. Although the first 50 eigenvectors account for 94% of eigenvectors on the systems 1 and 2, and 92% on system 3, the

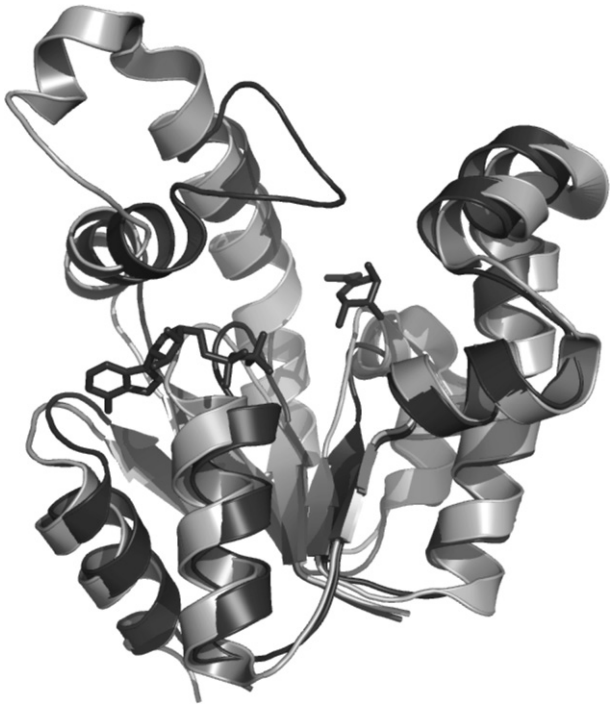

Figure 6. The binding of nucleotides, ADP or ATP, induces a rotational movement of the NB domain. The binding of SKM causes a rotation of the ESB domain. This motion is visible when we superposed the *Ba*SK apo-enzyme structure—template 2IYT—(light gray) to the *Ba*SK:ADP:SKM complex—template 2IYQ—(dark gray). The image was generated using Pymol.[58]

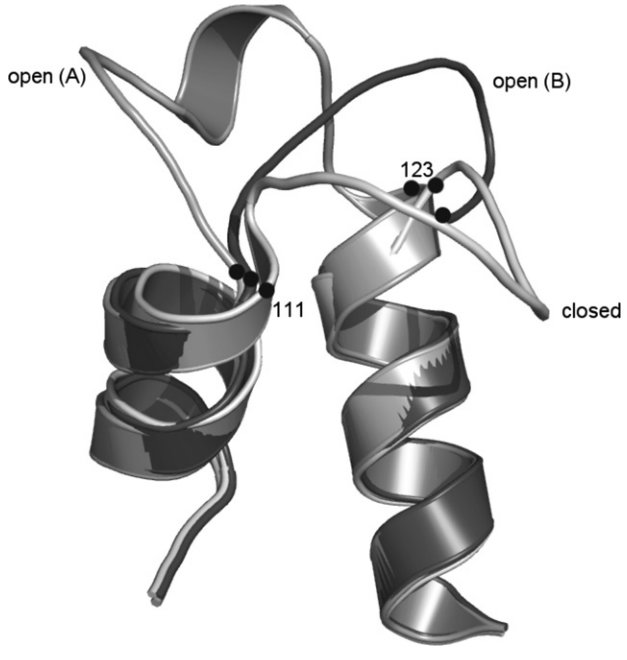

Figure 7. This figure illustrates the high flexibility of the LID domain, indicating by three different conformations. The image was generating using Pymol.[58]

first 4 eigenvectors alone represent about 67.1%, 66.0%, and 57.4% for uncomplexed (system 1 and 2, respectively) and complexed *Ba*SK (system 3), of the fluctuations. Thus, the displacements of the components of the first 4 eigenvectors for uncomplexed *Ba*SK (Open and closed LID domain) and *Ba*SK:SKM:ADP are shown in Fig. 12. For uncomplexed *Ba*SK, the significant fluctuations are

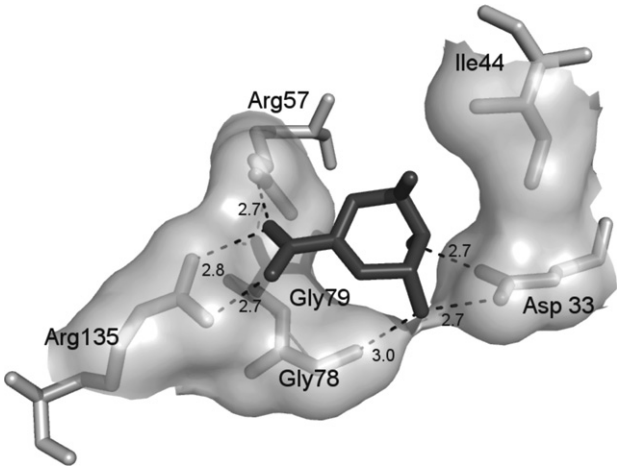

Figure 8. This image presents the active site of the *Ba*SK with SKM. The residues are presented in light gray and the SKM is presented in dark gray. The bond lengths are present in Å. The image was generated using Pymol.[58]

localized on the residues 1–16, 42–62, 106–36, and 150–166, as well as the C-terminal regions. It is not surprising that the significant fluctuations occur in these regions, because they are generally located in the loop regions of the protein. Similarly, there also exist the fluctuations in these regions for the complexed *Ba*SK. But the fluctuations in these residues decrease. Because the P-loop (1–14) moves toward the inhibitor and interacts with the ADP, the fluctuation in this region decreases. Correspondingly, the ESB (31–91) next to the P-Loop fluctuates less. Additionally, a significant fluctuation in residues 107–136, which are composed by LID domain, appears in the uncomplexed *Ba*SK.

For comparison of the fluctuations between uncomplexed and complexed *Ba*SK more clearly, we displayed the displacements of residues of eigenvector 1 for uncomplexed (Open and closed LID domain) and complexed *Ba*SK in one plot (Fig. 13), due to fluctuations of eigenvector 1 being the major motion. It can be seen from Fig. 13 that ligand-binding reduces motion in residues 1–16, 44 – 62, 103–109, 111–123, and 145–152, whereas increases fluctuations in segment 77–92. It is not surprising that the fluctuation in the LID reduces once the ligand binds, because the LID moves toward the ligand and forms hydrophobic interactions and hydrogen bonds with it, and the flexibility of the LID reduces accordingly.

3. Conclusions

The structures of *Ba*SK modeled in different conformational states provided snapshots of the interactions of this protein with its natural substrates. The comparison of the enzyme in apo-form to the complexes collaborate with a better understanding of the interactions between SK with its substrates. Structural analyses of *Ba*SK were able to identify the main residues involved in ATP- and SKM-binding, which are responsible for ligand-binding affinities. The residues involved in *Ba*SK- and *Mt*SK-binding sites do not differ significantly. The residues Asp33, Arg57, Gly78, and Gly79 present in *Ba*SK SKM-binding site are conserved in all SKs and also the residues Gly13 and Lys14 from the *Ba*SK ATP-binding site. S3P-binding involves conserved residues Lys14, Asp33, Arg57, and Gly78.

The 4 ns of MD simulations on three systems (two *Ba*SK uncomplexed and one *Ba*SK complexed with SKM and ADP), were carried out with the aim of revealing the possible mechanism of ligand recognition and inhibition. Based on our models, dynamics simulation and conformation analysis, many useful results were obtained. First, upon binding of the ligand, the flexibility of the *Ba*SK de-

Table 3
The residues involved in the ADP/ATP and SKM-binding sites

Protein(ligand)—LID conformation	Residues involved on binding pocket							
2IYQ(ADP)—closed	GLY12	GLY14	LYS15	SER16	THR17			
BaSK(ADP)—closed	GLY13	CYS65	TRP89	ARG109	VAL152			
2IYU(ADP)—open (A)	GLY12	GLY14	LYS15	SER16	THR17	ARG153		
BaSK(ADP)—open (A)	GLY11	GLY13	LYS14	*THR15*	THR16	ARG109	LYS 150	VAL152
2IYV(ADP)—open (B)	GLY12	GLY14	LYS15	SER16	THR17	ARG153		
BaSK(ADP)—open (B)	GLY11	GLY13	LYS14	*THR15*	THR16	ARG109	LYS150	VAL152
2IYW(ATP)—open (B)	GLY12	GLY14	LYS15	SER16	THR17	ARG153		
BaSK(ATP)—open (B)	GLY11	GLY13	LYS14	*THR15*	THR16	ARG109	LYS150	VAL152
2IYZ(ADP)—closed	GLY12	GLY14	LYS15	SER16	THR17	ARG110	ARG153	ARG155
BaSK(ADP)—closed	GLY13	*LYS14*	ARG109					
2IYQ(SKM)—closed	GLY80	ARG58	ARG136					
BaSK(SKM)—closed	ASP33	ILE44	ARG57	GLY78	GLY79	ARG135		
2IYR(SKM)—closed	ARG58	GLY80	ARG136					
BaSK(SKM)—closed	ASP33	ILE44	PHE48	ARG57	GLY78			
2IYS(SKM)—open (A)	ASP34	ILE45	ARG58	GLY80	GLY81	ARG136		
BaSK(SKM)—open (A)	ASP33	ILE44	ARG57	GLY78	GLY79	ARG135		

Open (A) and open (B) indicate two different conformations of the LID domain due to ligand binding. The mutations in the residues between template and model are pointed out in italic.

Table 4
Intermolecular hydrogen bonds between *Ba*SK/SKM and *Mt*SK/SKM

PROTEIN (template)	Ligand (SKM) atom	Protein (*Ba*SK) atom/residue	Distance (Å)
*Ba*SK (2IYQ)	O3	NH2/ ARG57	2.7
	O3	NH2/ ARG135	2.9
	O2	NH1/ ARG135	2.7
	O11	N/ GLY78	3.0
*Ba*SK (2IYR)	O11	N/ GLY78	3.1
	O3	NH2/ ARG57	2.7
*Ba*SK (2IYS)	O3	NH2/ ARG135	3.3
	O3	NH2/ ARG57	2.8
	O11	N/ GLY78	3.0
*Mt*SK (2IYQ)	O3	NH2/ ARG58	2.7
	O3	NH2/ ARG136	2.9
	O2	NH1/ ARG136	2.7
	O11	N/ GLY80	2.9
*Mt*SK (2IYR)	O11	N/ GLY80	3.1
	O2	NH1/ ARG136	2.9
	O3	NH2/ ARG136	3.1
	O3	NH2/ ARG58	2.7
*Mt*SK (2IYS)	O11	N/ GLY80	3.0
	O3	NH2/ ARG136	3.4
	O3	NH2/ ARG58	2.8

The first column presents the protein (*Ba*SK). In parentheses we show the *Mt*SK template used for modeling *Ba*SK. All these structures present the LID in closed conformation.

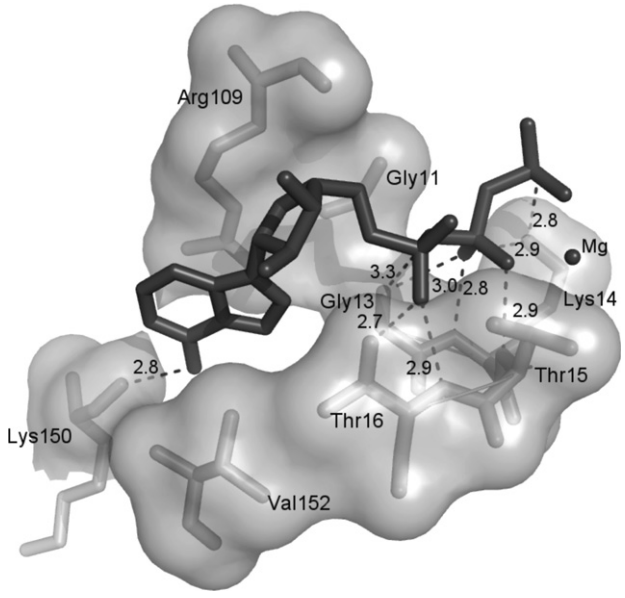

Figure 9. This image presents the active site of the *Ba*SK with ATP. The residues are presented in light gray and the ATP is presented in dark gray. The bond lengths are present in Å. The image was generated using Pymol.[58]

creases. The most notable change is the movement between the residues 44–62, 104–114, and 116–136, which are the residues present in the ESB, α6 and LID domains, respectively.

This study of the interaction between ligand and protein may help in the identification of new inhibitors for Shikimate Kinase, contributing for better understanding the catalytic activity and the rational drug design for the Shikimate Kinase from *B. anthracis*.

4. Materials and methods

4.1. Molecular modeling

Homology modeling is usually the choice method when there is a clear relationship of homology between the sequence of a target protein and at least one known structure. This computational technique is based on the assumption that tertiary structures of two proteins will be similar if their sequences were related, and it is the approach most likely to give the accurate results.[39] For modeling of the *Ba*SK we used as templates the structures of *Mt*SK deposited in the Protein Data Bank (PDB). Table 7 shows the PDB access codes for the templates and a description of the ligands, if present.

The web server PARMODEL[40] was used to modeling the enzyme in *apo* form and the complexes as well. PARMODEL is a parallelized version of the MODELLER.[41] All waters atomic coordinates were removed from the *Mt*SK structures to prepare the template structures. The modeling procedure begins with alignment of the

Table 5
pK_d values for ADP from the organisms *Bacillus anthracis*, *Escherichia coli*, *Erwinia chrysanthemi*, and *Methanococcus jannaschii*

Organism	X-SCORE	Experimental values (BRENDA)	PEARLS
Escherichia coli	4.6	3.7	4.6
Erwinia crysanthemi	4.4	4.1	3.6
Methanococcus jannaschii	4.8	3.4	4.5
Bacillus anthracis	5.3	—	6.4

All values are in pK_d units.

Table 6
Intermolecular hydrogen bonds between SK and SKM and the solvent contact surface (CS) from the organisms *Bacillus anthracis*, *Escherichia coli*, *Erwinia chrysanthemi*, and *Methanococcus jannaschii*

Organism	Ligand (SKM) atom	Protein (SK) atom/ residue	Distance (Å)	CS (Å^2)
Escherichia coli	O11	N/ GLY82	3.2	171
	O3	NH2/ARG60	3.3	
	O3	NH2/ARG140	2.8	
	O7	N2/LYS119	3.4	
Erwinia crysanthemi	O11	N/ GLY80	3.1	143
Methanococcus jannaschii	O2	NH2/ ARG48	2.9	166
	O2	NH2/ARG128	2.8	
Bacillus anthracis	O1	NH2/ ARG135	2.9	122
	O2	NH2/ARG135	2.9	
	O3	N/GLY78	2.8	
	O4	NH2/ARG57	2.7	

sequence to be modeled (target) with related known three-dimensional structures (templates). This alignment is usually the input to the program and the output is a three-dimensional model for the target sequence containing all main-chain and side-chain non-hydrogens atoms.[42] The alignment of *Ba*SK (target) and of *Mt*SK (template) is shown in Fig. 3.

Previous studies of *Mt*SK in complex with different ligands opened the possibility to assess the structure of SK in different instants during catalysis. The structural mechanism of the catalytic functioning of *Ba*SK was investigated on the basis of a series of high-resolution crystal structures from *Mt*SK, deposited in PDB, as templates, corresponding to individual steps in the enzymatic reaction.[9] The degree of primary sequence identity between *Mt*SK and *Ba*SK indicates that the crystallographic structures of the *Mt*SK are good models to be used as templates for *Ba*SK. A total of 1000 models were generated for each binary complex and the final models were selected based on objective function of the Modeller. All optimization process was performed on a Beowulf cluster with 16 nodes (BioComp, AMD Athlon XP 2100+, BioComp, Brazil).

4.2. Evaluation of binding affinity

Analysis of the interaction between a ligand and a protein target is still a scientific endeavor. The affinity and specificity between a ligand and its protein target depends on directional hydrogen bonds and ionic interactions, as well as on shape complementarity of the contact surfaces of both partners.[43] The program XSCORE[34] was used to evaluate the binding affinity of the ligands against *Mt*SK and *Ba*SK. According to this method, the binding affinity of the ligand can be decomposed to the contribution of individual atoms. Each ligand atom obtains a score, called the atomic-binding score, indicating its role in the binding process. The program reads the structure, assigns atom types and parameters, performs the calculation, and gives the dissociation constant of the given protein–ligand complex. The computational results are fed into a text file in which the detailed information of each ligand atom, including the atomic-binding score, is tabulated. These data were used to evaluate the affinities against SKs to verify possible resemblance in the structural basis for specificity against these enzymes.

4.3. Analysis of the models

The overall stereochemical quality of the final models for each enzyme of the *Ba*SK was assessed by the program PROCHECK.[44] Atomic models were superposed using the program LSQKAB from CCP4[37] and the intermolecular hydrogen bonds were assessed by the program LIGPLOT.[45] The cutoff for hydrogen bonds was 3.4 Å. Physico-chemical parameters of a protein such as isoeletric point, amino-acid, and atomic compositions were analyzed using PROTPARAM.[46]

4.4. Molecular dynamic simulations

MD simulations were performed with the GROMACS 3.3.1 package[47] using the Gromos 96.1 (43A2) force field. The SKM and ADP topologies were generated with the PRODRG program.[48] Accurate force field are essential for reproducing the conformational and

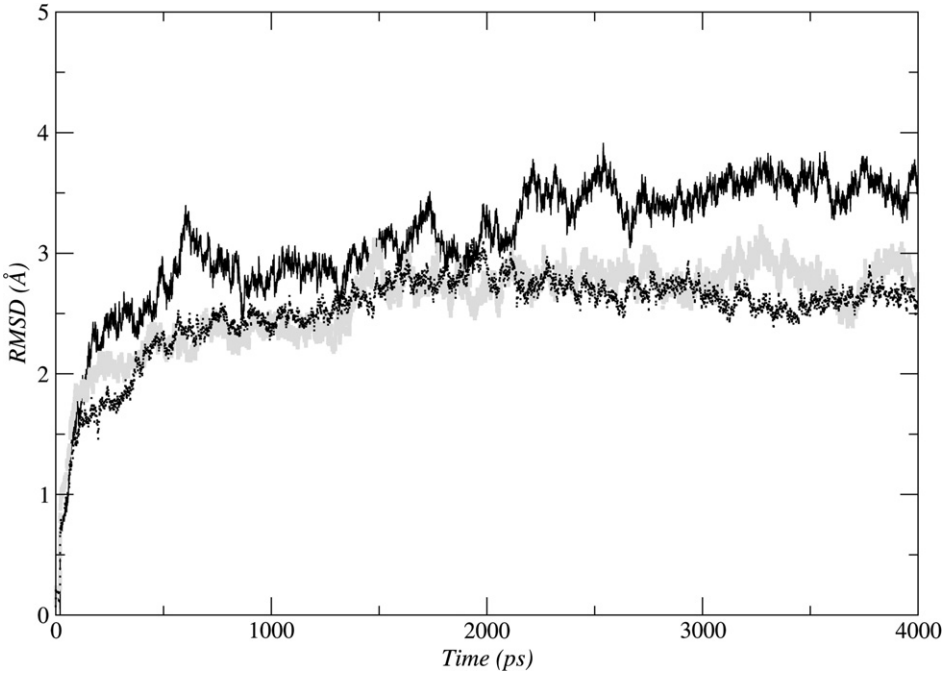

Figure 10. Graphical representation of root-mean-square deviation (RMSD) of all Cα from starting structure of models as a function of time. The solid black line represents RMSD of *Ba*SK unbound (Open LID domain—System 1), gray line represents *Ba*SK unbound (Closed LID domain—System 2), and dashed black line represents *Ba*SK:SKM:ADP (System 3).

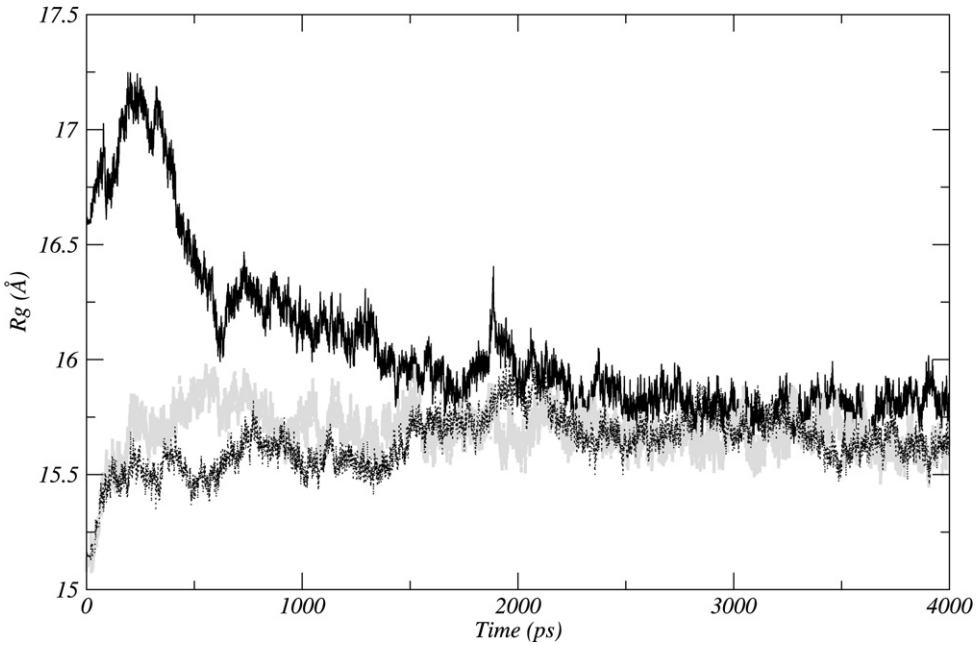

Figure 11. Radius of gyration as a function of time of uncomplexed *Ba*SK unbound Open LID domain (System 1) in black, *Ba*SK unbound Closed LID domain (System 2) in gray, and the *Ba*SK:SKM:ADP complex (System 3) in dashed line, during individual 4 ns MD simulation.

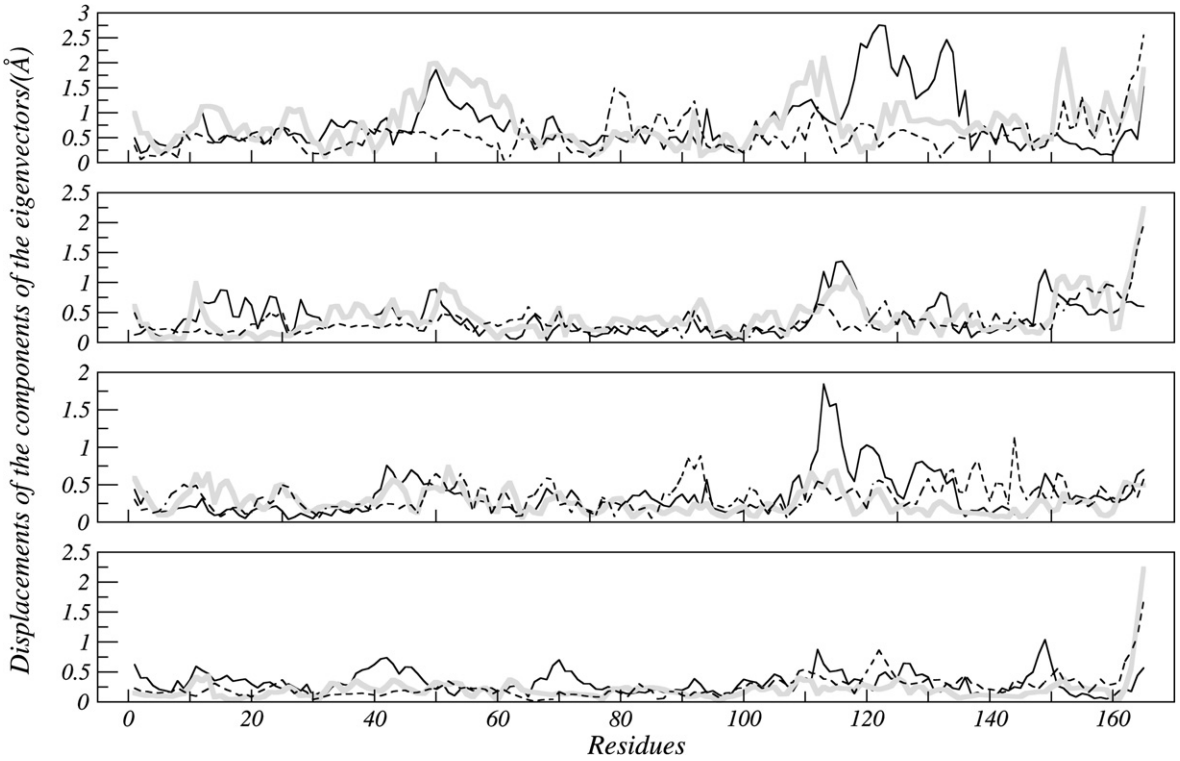

Figure 12. Displacements of the components of the first four eigenvectors black line for *Ba*SK unbound (Open LID domain—System 1), gray line *Ba*SK unbound (Closed LID domain—System 2), and dashed black line *Ba*SK:SKM:ADP (System 3).

dynamic behavior of condensed-phase systems, the Gromos 96.1 force fields well parameterized for proteins but the parameters for small molecules are still limited for simulations of more complicated biological systems, so the atomic charges in the SKM and ADP molecules were used GAMESS[49] which were submitted to single-point *ab initio* calculations at RHF 6-31G* level in order to obtain Löwdin derived charges. Manipulation of structures was performed with Swiss-PDBViewer v3.7 program.[50] The first system was composed by *Ba*SK in apo form with LID domain open (system 1), the second system by *Ba*SK in apo form with LID domain closed (system 2) and third system by *Ba*SK, SKM, and ADP (system 3). The simulations of the three systems were performed by a time period of 4 ns. In those systems were added Na+ counter ions (six Na+ ions on the systems 1 and 2 and ten Na+ ions on the

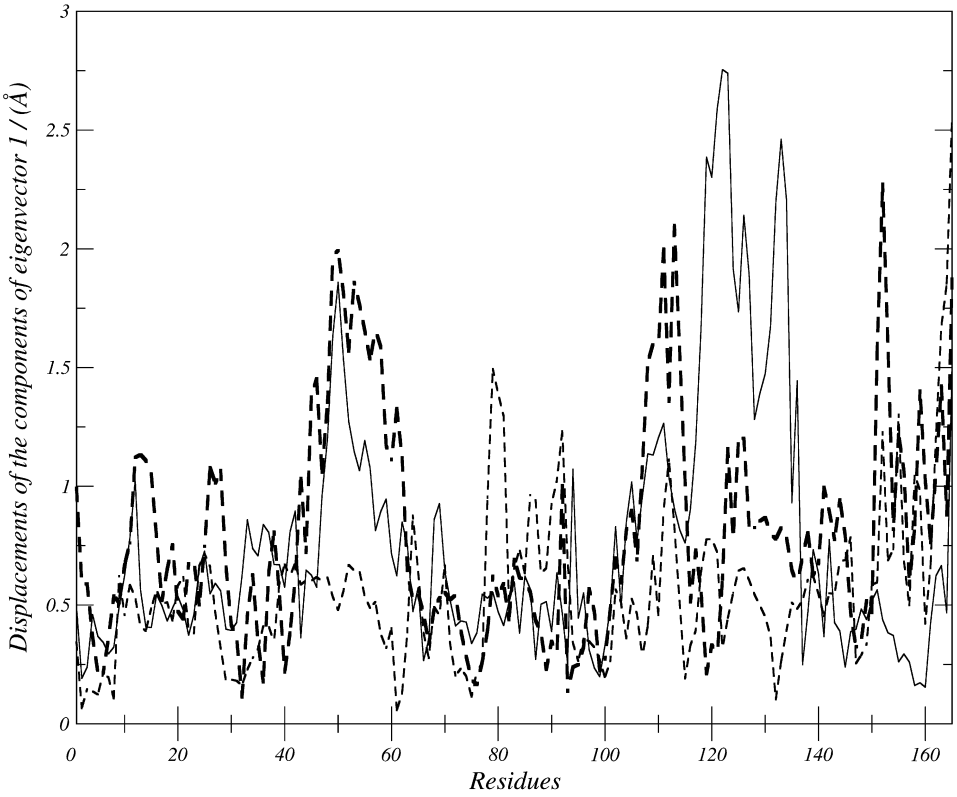

Figure 13. Displacements of the components of first eigenvector black line for *Ba*SK unbound (Open LID domain—System 1), gray line for *Ba*SK unbound (Closed LID domain—System 2), and dashed black line for *Ba*SK:SKM:ADP (System 3).

system 3) using *Genion* Program of the GROMACS simulation suite to neutralize the negative charge density of the systems. Each structure was placed in the center of a truncated cubic box filled with Extended Simple Point Charge (SPC/E) water molecules,[51] containing 12,985 for the system 1, 9249 for the system 2, and 9222 water molecules for the system 3. The initial simulation cell dimensions were 33.34, 48.70, 55.39 Å for the system 1, 41.92, 35.70, 45.14 Å for the system 2 and 3, and had the protein solvated by a layer of water molecules of at least 10 Å in all directions in both systems. During the simulations, bonds lengths within the proteins were constrained by using LINCS algorithm.[52] The SETTLE algorithm was used to constrain the geometry of water molecules.[53] In the MD protocol, all hydrogen atoms, ions, and water molecules were first subjected to 1500 steps of energy minimizations by steepest descent to remove close van der Waals contacts. The systems were then submitted to a short molecular dynamic with position restrains for a period of 20 ps and afterwards performed a full molecular dynamics without restrains. The temperature of the system was then increased from 50 to 300 K in 5 steps (50 to 100, 100 to 150, 150 to 200, 200 to 250, 250 to 300 K), and the velocities at each step were reassigned according to the Maxwell–Boltzmann distribution at that temperature and equilibrated for 10 ps except the last part of termalization phase where we used a period of 40 ps. Energy minimization and MD were carried out under periodic boundary conditions. The simulation was computed in the NPT ensemble at 300 K with the Berendsen temperature coupling and constant pressure of 1 atm with isotropic molecule-based scaling.[54] The LINCS algorithm, with a 10^{-5} Å tolerance, was applied to fix all bonds containing a hydrogen atom, allowing the use of a time step of 2.0fs in the integration of the equations of motion. No extra restrains were applied after the equilibration phase. The electrostatic interactions between non-ligand atoms were evaluated by the particle-mesh Ewald method[55] with a charge grid spacing of ~1.0 Å and the charge grid was interpolated on a cubic grid with the direct sum tolerance set to 1.0×10^{-5}. The Lennard–Jones interactions were evaluated using a 9.0 Å atom-based cutoff.[56] All analyses were performed on the ensemble of system configurations extracted at 0.5-ps time intervals from the simulation and MD trajectory collection was initiated after 1 ns of dynamics to guarantee a completely equilibrated evolution. The MD simulation and results analyses were performed on a personal computer Intel Core 2 Duo E6300 – 1.86GHz and 4Gb RAM. The convergence of the different simulations were analyzed in terms of the secondary structure, root mean-square deviation (RMSD) from the initial models structures and radius of gyration (Rg).

4.5. Essential dynamics analysis

Essential Dynamics (ED), also known as principal component analysis (PCA), is a method commonly used for dissecting the dynamics of proteins and their importance in biological processes, like protein folding or substrate binding. The ED analysis is a technique that reduces the complexity of the data and extracts the concerted motion in simulations that are essentially correlated and presumably meaningful for biological function.[57] In the ED analysis, a variance/covariance matrix was constructed from the trajectories after removal of the rotational and translational movements. A set of eigenvectors and eigenvalues was identified by diagonalizing the matrix. The eigenvalues represented the amplitude of the eigenvectors along the multidimensional space, and the displacements of atoms along each eigenvector showed the concerted motions of protein along each direction. An assumption of ED analysis is that the correlated motions for the function of the protein are described by eigenvectors with large eigenvalues. The movements of protein in the essential subspace were identified by projecting the

Table 7
PDB access codes, resolution, description of the ligands and the LID conformation for *Mt*SK structures (templates)

Enzyme	PDB access code	Resolution (Å)	Ligands	LID conformation
SK	1WE2	2.3	SKM + ADP	Closed
	2IYT	1.5	Apo	Open (A)
	2IYU	1.8	ADP	Open (A)
	2IYV	1.3	ADP	Open (B)
	2IYW	1.8	MgATP	Open (B)
	2IYS	1.4	SKM	Open (A)
	2IYR	2.0	SKM	Closed
	2IYQ	1.8	SKM + ADP	Closed
	2IYY	1.6	S3P + SO_4	Closed
	2IYZ	2.3	S3P + ADP	Closed
	1L4Y	2.0	MgADP	Closed

Open (A) and open (B) indicate two different conformations of the LID domain due to ligand binding.

Cartesian trajectory coordinates along the most important eigenvectors from the analysis.

Acknowledgement

This work was supported by grants from Millennium Institute (CNPq-MCT). WFA is a researcher from the National Research Council of Brazil (CNPq).

Supplementary data

Supplementary data associated with this article can be found, in the online version, at doi:10.1016/j.bmc.2008.07.051.

References and notes

1. Mock, M.; Fouet, A. *Annu. Rev. Microbiol.* **2001**, *55*, 647.
2. Kalamas, A. G. *Anesthes. Clin. North Am.* **2004**, *22*, 533.
3. Bagget, H. C.; Rhodes, J. C.; Fridkin, S. K.; Quinn, C. P.; Hageman, J. C.; Friedman, C. R.; Dykewicz, C. A.; Semenova, V. A.; Romero-Steiner, S.; Elie, C. M.; Jernigan, J. A. *Clin. Infect. Dis.* **2005**, *41*, 991.
4. Jernigan, D. B.; Raghunathan, P. L.; Bell, B. P.; Brechner, R.; Bresnitz, E. A.; Butler, J. C.; Cetron, M.; Cohen, M.; Doyle, T.; Fischer, M.; Greene, C.; Griffith, K. S.; Guarner, J.; Hadler, J. L.; Hayslett, J. A.; Meyer, R.; Petersen, L. R.; Phillips, M.; Pinner, R.; Popovic, T.; Quinn, C. P.; Reefhuis, J.; Reissman, D.; Rosenstein, N.; Schuchat, A.; Shieh, W. J.; Siegal, L.; Swerdlow, D. L.; Tenover, F. C.; Traeger, M.; Ward, J. W.; Weisfuse, I.; Wiersma, S.; Yeskey, K.; Zaki, S.; Ashford, D. A.; Perkins, B. A.; Ostroff, S.; Hughes, J.; Fleming, D.; Koplan, J. P.; Gerberding, J. L. *Emerg. Infect. Dis.* **2002**, *8*, 1019.
5. Sanderson, W. T.; Stoddard, R. R.; Echt, A. S.; Piacitelli, C. A.; Kim, D.; Horan, J.; Davies, M. M.; McCleery, R. E.; Muller, P.; Schnorr, T. M.; Ward, E. M.; Hales, T. R. *J. Appl. Microbiol.* **2004**, *96*, 1048.
6. Casadevall, A. *Front. Biosci.* **2008**, *13*, 4009.
7. Oliveira, J. S.; Sousa, E. H. S.; Basso, L. A.; Palaci, M.; Dietze, R.; Santos, D. S.; Moreira, I. S. *Chem. Commun.* **2004**, *7*, 312.
8. Oliveira, J. S.; Sousa, E. H. S.; Souza, O. N.; Moreira, I. S.; Santos, D. S.; Basso, L. A. *Curr. Pharm. Des.* **2006**, *12*, 2409.
9. Oliveira, J. S.; Vasconcelos, I. B.; Moreira, I. S.; Santos, D. S.; Basso, L. A. *Curr. Drug Targets* **2007**, *8*, 399.
10. Dias, M. V.; Vasconcelos, I. B.; Prado, A. M.; Fadel, V.; Basso, L. A.; de Azevedo, W. F., Jr.; Santos, D. S. *J. Struct. Biol.* **2007**, *159*, 369.
11. Vasconcelos, I. B.; Meyer, E.; Sales, F. A. M.; Moreira, I. S.; Basso, L. A.; Santos, D. S. *Anti-infective Agents Med. Chem.* **2008**, *7*, 50.
12. Tipparaju, S. K.; Jovasawal, S.; Forrester, S.; Mulhearn, D. C.; Pegan, S.; Johnson, M. E.; Mesecar, A. D.; Kozikowski, A. P. *Bioorg. Med. Chem. Lett.* **2008**, *18*(12), 3565.
13. Pereira, J. H.; Vasconcelos, J. B.; Oliveira, J. S.; Caceres, R. A.; de Azevedo, W. F., Jr.; Basso, L. A.; Santos, D. S. *Curr. Drug Targets* **2007**, *8*, 459.
14. Dias, M. V.; Faím, L. M.; Vasconcelos, I. B.; de Oliveira, J. S.; Basso, L. A.; Santos, D. S.; de Azevedo, W. F., Jr. *Acta Crystallogr. Sect. F Struct. Biol. Crystallogr. Commun.* **2007**, *63*, 1.
15. Silveira, N. J.; Uchôa, H. B.; Pereira, J. H.; Canduri, F.; Basso, L. A.; Palma, M. S.; Santos, D. S.; de Azevedo, W. F., Jr. *J. Mol. Model.* **2005**, *11*, 160.
16. Pereira, J. H.; de Oliveira, J. S.; Canduri, F.; Dias, M. V.; Palma, M. S.; Basso, L. A.; Santos, D. S.; de Azevedo, W. F., Jr. *ActaCrystallogr. D Biol. Crystallogr.* **2004**, *60*, 2310.
17. Segura-Cabrera, A.; Rodríguez-Pérez, MA. *Bioorg. Med. Chem. Lett.* **2008**, *18*, 3152.
18. Bentley, R. Crit. Ver. *Biochem. Mol. Biol.* **1990**, *25*, 307.
19. Davies, G. M.; Barret-Bee, K. J.; Jude, D. A.; Lehan, M.; Nichols, W. W.; Pinder, P. E.; Thain, J. L.; Watkins, W. J.; Wilson, R. G. *Antimicrob. AgentsChemother.* **1994**, *38*, 403.
20. De Azevedo, W. F. *Curr. Drug Targets* **2007**, *8*, 387.
21. Pereira, J. H.; Canduri, F.; de Oliveira, J. S.; da Silveira, N. J. F.; Basso, L. A.; Palma, M. S.; De Azevedo, W. F.; Santos, D. S. *Biochem. Biophys. Res. Commun.* **2003**, *312*, 608.
22. Arcuri, H. A.; Borges, J. C.; Fonseca, I. O.; Pereira, J. H.; Neto, J. R.; Basso, L. A.; Santos, D. S.; de Azevedo, W. F., Jr. *Proteins* **2008**, *72*, 720.
23. Marques, M. R.; Pereira, J. H.; Oliveira, J. S.; Basso, L. A.; de Azevedo, W. F., Jr.; Santos, D. S.; Palma, M. S. *Curr. Drug Targets* **2007**, *8*, 445.
24. Borges, J. C.; Pereira, J. H.; Vasconcelos, I. B.; dos Santos, G. C.; Olivieri, J. R.; Ramos, C. H.; Palma, M. S.; Basso, L. A.; Santos, D. S.; de Azevedo, W. F., Jr. *Arch. Biochem. Biophys.* **2006**, *452*, 156.
25. Dias, M. V.; Borges, J. C.; Ely, F.; Pereira, J. H.; Canduri, F.; Ramos, C. H.; Frazzon, J.; Palma, M. S.; Basso, L. A.; Santos, D. S.; de Azevedo, W. F., Jr. *J. Struct. Biol.* **2006**, *154*, 130.
26. Basso, L. A.; da Silva, L. H.; Fett-Neto, A. G.; de Azevedo, W. F., Jr.; Moreira, Ide. S.; Palma, M. S.; Calixto, J. B.; Astolfi, F. S.; dos Santos, R. R.; Soares, M. B.; Santos, D. S. *Mem. Inst. Oswaldo Cruz* **2005**, *100*, 475.
27. Ely, F.; Nunes, J. E.; Schroeder, E. K.; Frazzon, J.; Palma, M. S.; Santos, D. S.; Basso, L. A. *BMC Biochem.* **2008**, *29*, 9.
28. De Azevedo, W. F.; Canduri, F.; de Oliveira, J. S.; Basso, L. A.; Palma, M. S.; Pereira, J. H.; Santos, D. S. *Biochem. Biophys. Res. Commun.* **2002**, *295*, 142.
29. Parish, T.; Stoker, N. G. *Microbiology* **2002**, *148*, 3069.
30. Vonrhein, C.; Schlauderer, G. J.; Schulz, G. E. *Structure* **1995**, *3*, 483.
31. Hartmann, M. D.; Bourenkov, G. P.; Strizhov, A. O. N.; Bartunik, H. D. *J. Mol. Biol.* **2006**, *364*, 411.
32. Caceres, R. A.; Macedo Timmers, L. F.; Vivan, A. L.; Schneider, C. Z.; Basso, L. A.; De Azevedo, W. F., Jr.; Santos, D. S. *J. Mol. Model.* **2008**, *14*, 427.
33. Schomburg, I.; Chang, A.; Ebeling, C.; Hofmann, O.; Ebeling, C.; Ehrentreich, F.; Schomburg, D. *Trends Biochem. Sci.* **2002**, *27*, 54.
34. Wang, R.; Liu, L.; Lai, L.; Tang, Y. *J. Mol. Model.* **1998**, *4*, 379.
35. Han, L. Y.; Lin, H. H.; Li, Z. R.; Zheng, C. J.; Cao, Z. W.; Xie, B.; Chen, Y. Z. *J. Chem. Inf. Model.* **2006**, *46*, 445.
36. Lee, B.; Richards, F. M. *J. Mol. Biol.* **1971**, *55*, 379.
37. Collaborative Computation Project, Number 4. *Acta Crystallogr. D Biol. Crystallogr.* **1994**, *50*, 760.
38. Liu, G.; Tan, J.; Niu, C.; Shen, J.; Luo, X.; Shen, X.; Chen, K.; Jiang, H. *Acta Pharm. Sin.* **2006**, *27*, 100.
39. Kroemer, R. T.; Doughty, S. W.; Robinson, A. J.; Richards, W. G. *Protein Eng.* **1996**, *9*, 493.
40. Uchoa, H. B.; Jorge, G. E.; Da Silveira, N. J. F.; Camera, J. C.; Canduri, F.; De Azevedo, W. F. *Biochem. Biophys. Res. Commun.* **2004**, *325*, 1481.
41. Sali, A.; Blundell, T. L. *J. Mol. Biol.* **1993**, *234*, 779.
42. Canduri, F.; Uchoa, H. B.; De Azevedo, W. F., Jr. *Biochem. Biophys. Res. Commun.* **2004**, *324*, 661.
43. De Azevedo, W. F.; Mueller-Dieckmann, J. H.; Schulze-Gahmen, U.; Worland, P. J.; Sausville, E.; Kim, S. H. *Proc. Natl. Acad. Sci. U.S.A.* **1996**, *93*, 2735.
44. Laskowski, R. A.; Macarthur, M. W.; Moss, D. S.; Thornton, J. M. *J. Appl. Crystallogr.* **1993**, *26*, 283.
45. Wallace, A. C.; Laskowski, R. A.; J.M.Thornton *Protein Eng.* **1995**, *8*, 127.
46. Gasteiger, E.; Hoogland, C.; Gattiker, A.; Duvaud, S.; Wilkins, M. R.; Appel, R. D.; Bairoch, A. In *The Proteomics Protocols Handbook*; Walker, John M., Ed.; Humana Press, 2005; p 571.
47. Van der Spoel, D.; Lindahl, E.; Hess, B.; Groenhof, G.; Mark, A. E.; Berendsen, H. J. C. *J. Comput. Chem.* **2005**, *26*, 1701.
48. Van Aalten, D. M. F.; Bywater, B.; Findlay, J. B. C.; Hendlich, M.; Hooft, R. W. W.; Vriend, G. *J. Comput. Aided Mol. Des.* **1996**, *10*, 255.
49. Schmidt, M. W.; Baldridge, K. K.; Boatz, J. A.; Elbert, S. T.; Gordon, M. S.; Jensen, J. H.; Koseki, S.; Matsunaga, N.; Nguyen, K. A.; Su, S. J.; Windus, T. L.; Dupuis, M.; Montgomery, J. A. *J. Comput. Chem.* **1993**, *14*, 1347.
50. Guex, N.; Peitsch, M. C. *Electrophoresis* **1997**, *18*, 2714.
51. Berendsen, H. J. C.; Postma, J. P. M.; van Gunsteren, W. F.; Hermans, J. In *Intermolecular Forces*; Pullman, B., Ed.; Reidel D. Publishing Company: Dordrecht, The Netherlands, 1981; p 331.
52. Hess, B.; Bekker, H.; Berendsen, H. J. C.; Fraaije, J. G. E. M. *J. Comput. Chem.* **1997**, *18*, 1463.
53. Miyamoto, S.; Kollman, P. A. *J. Comput. Chem.* **1992**, *13*, 952.
54. Chowdhuri, S.; Ming-Liang, T.; Ichiye, T. *J. Chem. Phys.* **2006**, *125*, 144513.
55. Darden, T.; York, D.; Pedersen, L. A. *J. Chem. Phys.* **1993**, *98*, 10089.
56. De Souza, O. N.; Ornstein, R. L. *J. Biomol. Struct. Dyn.* **1999**, *16*, 1205.
57. Amadei, A.; Linssen, A. B. M.; Berendsen, H. J. C. *Proteins* **1993**, *17*, 412.
58. Delano, W. L.; Lam, J. W. *Abstr. Pap. Am. Chem. Soc.* **2005**, *230*, 1371.